

Development of an Advanced Optical Coherence Tomography System for Radiation Dosimetry

Masoumeh Hoseinnezhad¹, Mohammad Mahdavi¹, Seyyed Rabee Mehdi Mahdavi^{2*}

1. Department of Physics, University of Mazandaran, Babolsar, Iran

2. Radiation Biology Research Center, Department of Medical Physics, Iran University of Medical Sciences, Tehran, Iran

ARTICLE INFO

Article type:
Original Article

Article history:
Received: Oct 31, 2017
Accepted: Mar 11, 2018

Keywords:
Charges Coupled Device
Optical Coherence
Tomography Magnetic
Resonance Imaging
Gels Radiometry
Dose

ABSTRACT

Introduction: According to the literature, optical coherence tomography (OCT) can be used measure radiation absorbed dose. This study was carried out to design a computed tomography system for the calculation of absorbed dose and optimization of dose delivery in radiotherapy using gel dosimeters.

Material and Methods: An advanced charge-coupled device based OCT system was developed in laboratory with the capability for high resolution three-dimensional (3D) radiation dosimetry using gel dosimeters. The OCT system was compared to magnetic resonance imaging (MRI) as a standard system to investigate its accuracy. Additionally, a number of parameters were checked for assessing the performance of the system.

Results: Developing an advanced OCT system, the calibration curve was drawn for OCT and MRI and the received dose values were compared. The amounts of dose obtained from OCT and MRI were 1.98 and 2 Gy respectively with a relative difference of 2%.

Conclusion: The quality of treatment can be improved using OCT system in radiotherapy dosimetry.

► Please cite this article as:

Hoseinnezhad M, Mahdavi M, Mahdavi SRM. Development of an Advanced Optical Coherence Tomography System for Radiation Dosimetry. Iran J Med Phys 2018; 15: 243-250. 10.22038/ijmp.2018.27121.1279.

Introduction

There are several techniques for gel dosimetry. Magnetic resonance imaging (MRI) and optical coherence tomography (OCT) are two important three-dimensional (3D) dose distribution modalities [1-4]. It is now a decade since the first OCT images of a polymer gel introduced [5]. Thereafter, there have been considerable advances in both 3D imaging techniques and dosimeter formulation. OCT systems are very useful for determining the amount of dose in the techniques for delivering radiation therapy such as intensity-modulated radiation therapy.

The initial OCT systems that provided good results were based on laser as a light source and photodiode detectors. An important advantage of these systems scan time reduction [6]. Gore et al. in 1996 provided the first generation of OCT systems as a new scanning system for tissue equivalent gel dosimeters [7].

This nearly accurate and reliable system was based on helium-neon laser with the wavelength of 632 nm; and used to obtain the data of each projection (De Deene et al., 1998; Hilts et al., 2000; Mather and Baldock, 2003). More recently, other approaches to OCT scanning system have been proposed including scanning broad-beam systems [8-12]

This system has high spatial resolution and low scanning time. Generally, the scanning laser systems

are used for dosimetry, where the primary contrast mechanism is light scattering (e.g. polymer gels). Newer systems are those using light-emitting diode (LED), as a light source, and a charge-coupled device (CCD), as a detector.

This study was conducted to design and construct an OCT. Additionally, we tried to compare the accuracy of this system with MRI.

Materials and Methods

In Figure 1, the schematic of OCT scanner designed in the Department of Physics, Mazandaran University, Babolsar, and Radiation Biology Research Center, Department of Medical Physics, Iran University of Medical Sciences, Tehran, Iran, in 2017 is shown. The different parts of this system are listed in Table 1. Several improvements in scanner design were incorporated into this work. To expand the collimated beam to a larger one, we used the beam expander. Moreover, the CCD was used to diminish the scanning time and remove transferred motions at each stage.

The schematic of optical-CT scanner designed in labs. of Physics Department of Mazandaran University and radiation biology research center, Medical Physics Department of Iran University of Medical Sciences in 2017 is shown in Fig. 1. Different parts of this system

*Corresponding Author: Tel: +98 021 35302491; Fax: +98 021 35302480; Email: M.mahdavi@umz.ac.ir

are listed in table 1. Several improvements in scanner design were incorporated for this work. We used the beam expander because the collimated light was expanded better. Also the CCD was used for decreasing time scan. The CCD removes transferred motions in every stage and considerably decreases the time scan.

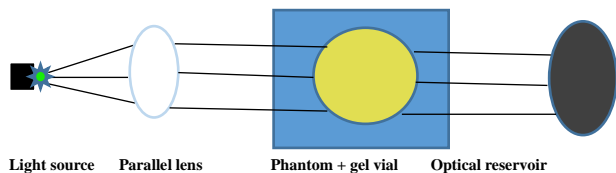


Figure 1. Schematic of optical coherence tomography system

The roles of different parts of the system are explained one by one as follows;

Light source (light-emitting diode)

In this study, monochromatic green LEDs with the wavelength of 532 nm were utilized.

Therefore, the uniform backlight was green filtered to match the maximum sensitivity of the

radiochromic response at 532 nm. The human eye is not capable of seeing the wavelengths outside of the visible range; therefore, they are not suitable for radiation. Moreover, the human eye is more sensitive to several specific wavelengths of the visible spectrum (Figure 2).

The eye sensitivity function is determined by the luminosity function, which is the average spectral sensitivity of human visual perception of brightness. The optical effect describes that which fraction of the electromagnetic power is appropriate to illuminate the environment. This number is obtained through dividing the flux over the radiant flux. An optical wavelength outside the visible spectrum has low optical effect due to its own radiant power spectrum; however, its light power is zero.

The wavelengths close to the maximum sensitivity of the eye are more effective in optical efficiency than those within the visible range. In the International Devices of Universities whose optical output is measured in lumens per watt (lm/W), the maximum optical effect in the bright environment can be 683 lm/W in single light and at 555 nm (green). In dark conditions, the maximum optical output can be increased to 1700 lm/W at the wavelength of 507 nm.

Table 1. Different parts of optical coherence tomography system

| 1 | 2 | 3 | 4 | 5 | 6 | 7 |
|------------------------------------|---------------|------------|----------|------------|--|--------------|
| Light source(light-emitting diode) | Beam expander | Water bath | Gel vial | Step motor | Optical reservoir(charge-coupled device) | Capture card |

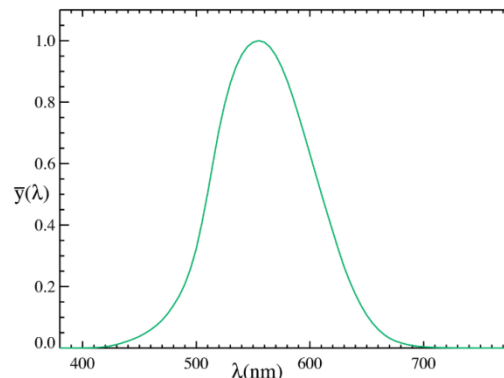


Figure 2. The sensitivity of the human eye to light, according to the standards of The International Commission on Illumination standard in 1924 (The horizontal axis represents the wavelength [nm])[13]

Considering the above interpretation, the green light of LED with the wavelength of 532 nm was suitable for our imaging purposes. To repair the light leak, the LED was placed in an aluminum tube with a pinhole at one end. A spatial filter with the diameter of 1 mm was placed in front of the LED lamp. Due to the high light intensity of the camera pixels and the lack of uniformity of the optical field, a diffuser was used.

This diffuser can reduce the light intensity and increase the uniformity of the field of light. Furthermore, it is tangent to the light source in a range of 2 to 3 mm filters. The light of LED irradiates to beam expander. A layout was considered to collimate the exited light beam (Figure 1) (Hunt and Pointer, 2011; Ikeda and Nakano, 1986).

Beam expander

Beam expander is a tube containing two lenses, one of which is a collimator lens and the other is an expander lens. It is an application requirement in case of using light sources and optics. Therefore, we used a combination of spatial filter and beam expander with specialized expansion ratio. The output of the light source was on the order of 1 mm or so. Larger beam diameters are vital for communication applications. In addition, expanded beam is required to improve beam focusing in material processing applications.

Water bath

Perspex material with near water equivalent density was used as the water bath to deviate the beam with less angle of refraction after contacting with sample. The length, width, and height of this phantom were 30 cm, 15 cm, and 12 cm, respectively.

Gel vial

This vial is a cylindrical container that contains gel, which is connected to the stepper motor and placed in the water phantom.

Stepper motor

Stepper motor makes vial rotation possible by 1° in each 1 s step.

1. Optical reservoir (charge-coupled device)

There are two types of OCT systems based on the optical reservoir, namely, photo diode detector- and CCD detector-based OCTs. The advantages of photo diode detector-based systems are the small size of photosensitive surface that allows to detect approximately all scattered ray as well as less contortion and artifact in the image reconstruction. However, the use of these systems is time-consuming because all of the transferred and rotational movements are repeated in every projection.

Nevertheless, the CCD-based systems receive scattered rays and diminish the scanning time by eliminating the transferred movements. The CCD-based system used in this study was made in Mintron Enterprise Co., Ltd, Taipei, Taiwan. The size of the sensor was 582×753 pixels and the signal-to-noise ratio was 58 dB.

Capture card

Capture card is a tool used to convert the physical quantities to digital numbers, which determine the amplitude of those quantities. In the OCT systems, a coaxial cable connects the CCD to the capture card to convert the produced raw images to digital numbers. This card is connected to the computer and transfers digital numbers to the computer memory. The capture card used in the current study was made in Taiwan.

Set up of the system

First, the light source assembly was connected to a holder, put on the optical base, and screwed to one edge of the optical board. According to our physical calculations, the beam expander was placed within a

distance of 10 cm from the light source. Therefore, the first lens of the beam expander gave us a beam of wide light, and the second lens, located in the center of the lens, created a perfectly collimated light.

The water phantom was placed at a distance of about 5 cm from the beam expander, and the vial of gel was placed inside this water phantom. In order to put the vial of gel into the phantom, we designed and constructed a frame that was moved from the point of view and mounted a shaft to hold the vial.

The shaft was designed to rotate in the direction of the sample axis at all angles and was connected to a stepper motor that rotated the gel vial with the degree of turning. An optical receiver in front of the light source is required to receive the beam hitting the vial. Accordingly, a CCD optical receiver was put at a distance of 5 cm from the phantom and just opposite the light source. The CCD used in this study was produced by the Mintron Enterprise Co. with the signal-to-noise ratio of 58 dB. The images provided to the CCD were raw, and thus we used a capture card to convert these raw values to digital numbers. This card was mounted on the computer and connected to the CCD with a coaxial cable. The final layout of the OCT system is demonstrated in Figure 3.

Evaluation of the Optical Coherence Tomography System Parameters

It is possible to assess the function of the system by evaluating several parameters such as spatial resolution, the effect of the number of projection, non-uniformity, and repeatability.

Spatial resolution

Spatial resolution is the capability of the imaging system to separate closely spaced details. There are several methods for the evaluation of spatial resolution. Here, the method for measuring the modulation transfer function (MTF) is briefly described. MTF is a quantity in optics that shows the output contrast changes as blurred of point spread function (PSF).

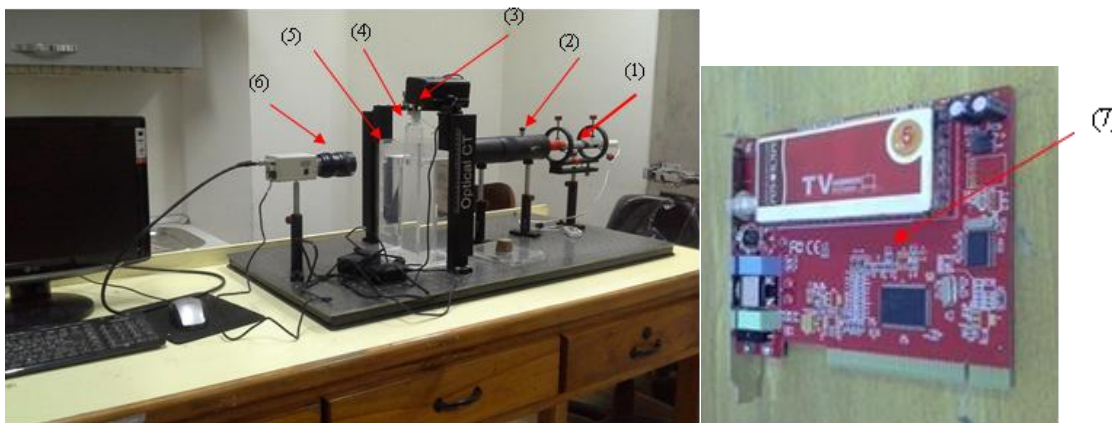


Figure 3.The final layout of the optical coherence tomography system
 1) light source 2) beam expander 3) stepper motor 4) gel vial 5) water phantom 6) CCD 7) capture card

Each system has response in front of a real beat function (i.e., point source), and it produces an output or image that determines the characteristics of the system by convolution.

In other words, the system response to the PSF is due to the effect of a system on a bitwise or PSF that occurs as a fading signal or image (without sharpness or edge) at the location or time dimension. In this method, first, a high-contrast sample such as a metal wire with the smallest possible diameter is scanned by OCT system. Thereafter, the sample function graph was plotted in terms of the pixel value of the image and the sample location.

In addition, the MTF was obtained from the Fourier transform of the PSF, according to which 10% of the graph represented the spatial resolution of the system. A 0.25-mm-diameter wire was placed in the center of the vial to determine the post-scanning spatial resolution of the system. As demonstrated in Figure 4 10% of the graph was equal to 3.6 cycle/mm, which means that the spatial resolution of the system was 0.27 mm, and this system could detect objects smaller than 1 mm and separate distances less than 1 mm.

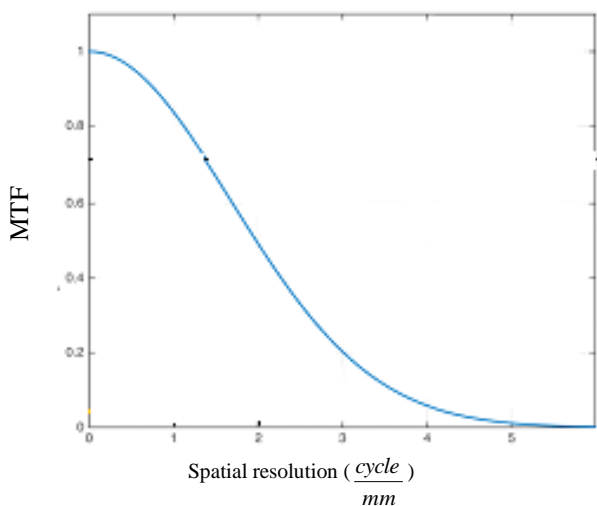


Figure 4. Modulation transfer function for a 0.25-mm-diameter wire

Checking the Effect of the Number of Projection

To investigate the effect of the number of projections (the angles of rotation of the motor) on the accuracy and precision of the image, a sample of 0.25 mm was scanned at different angles. After the projections were reconstructed, sectional images were taken and finally a 3D image of the sample was obtained. First, the rotation was done at 1° and 360 projections were achieved. By increasing the rotation angles to 4°, 16°, 35°, 45°, and 90° and subsequently reducing the number of projections, the same sample was scanned again. The wire size in all cross-sectional images is demonstrated in Table 2.

Table 2. Sample size measured in various projections

| The real size of sample | Sample size measured (mm) | Angle (degree) | Projections number |
|-------------------------|---------------------------|----------------|--------------------|
| 0.25 | 0.25 | 1 | 360 |
| 0.25 | 0.25 | 4 | 200 |
| 0.25 | 0.25 | 16 | 100 |
| 0.25 | 0.23 | 35 | 24 |
| 0.25 | 0.22 | 45 | 12 |
| 0.25 | 0.19 | 90 | 8 |

Non-uniformity

To determine the uniformity of the system, homogeneous such as MAGIC-f gel should be used to smooth the light. Five regions of interest (ROI) circles in the central slice of 400 pixels were selected, one in the center and four in the peripheral areas (Figure 5). The non-uniformity was obtained according to Equation 1.

$$Non - uniformity = \frac{MGV_{centre} - MGV_{around}}{MGV_{around}} \times 100 \tag{1}$$

In this equation, MGV represents the ROI points. The non-uniformity less than 10% indicated that the uniformity of the system was within the acceptable range. In this study, non-uniformity was 8%. We scanned a cross-sectional image of the gel vial and obtained the cut profile using the MATLAB software. Regarding our calculations, the uncertainty level of the system was 1.5733, which was acceptable.

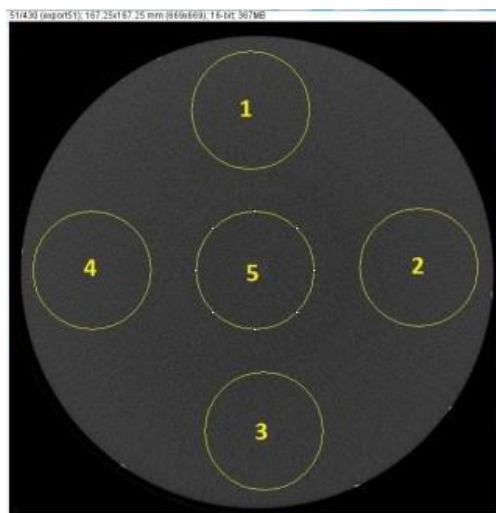


Figure 5. Five regions of interest for uniformity

Repeatability

Repeatability means the same results obtained in the same conditions and with the same methods, equipment and, operator on similar samples. The repeatability limit is the amount that we expect the difference between two test results obtained under repetitive conditions with a probability of less than or equal to 95% that obtained by Equation 2:

$$r_{testmethod} = 0.2802x^{0.07901} \tag{2}$$

Table 3. Protocol for gel preparation

| Material | Operation in gel | Chemical formula | Value (ml or g) |
|--------------------|------------------|---------------------|-----------------|
| Gelatin | Gel agent | $C_4H_{11}NO_3.HCl$ | 82 g |
| Ascorbic acid | Antioxidant | $C_6H_8O_6$ | 0.352 g |
| Formaldehyde (37%) | Polymerization | HCHO | 30 ml |
| Copper(II) sulfate | Catalyzer | $CuSO_4$ | 20 mg |
| Methacrylic acid | Monomer | $CH_2:C(CH_3)COOH$ | 50 g |
| Pure water | Solvent | H_2O | 810 ml |

x'' is considered as the repeatability limit. To determine the repeatability of the system, a gel vial was scanned twice with the OCT system in the same conditions. The difference between the two readings was 0.96, which demonstrated that this test was 96% repeatable.

Preparation of the gel

The protocol of the preparation of 1000 g of the MAGIC-f gel, used in this study, is shown in Table 3. As demonstrated in the mentioned table, 810 ml of pure water was poured in a vessel and gelatin was added to the water in laboratory temperature. The water and gelatin were heated to 45°C and were riled simultaneously by magnet until the gelatin was entirely dissolved. After half an hour, we turned off the heater. When the temperature reached to 35°C, we added ascorbic acid, $CuSO_4$, and formaldehyde to the mixture, and after 5 min, methacrylic acid was added. The $CuSO_4$ and ascorbic acid were solved in 5 ml of water separately and were added to the mixture. This solution was poured in vials, and they were kept in the refrigerator at the temperature of 10°C for a day. Thereafter, the vials were sent to radiotherapy center for irradiation.

Irradiation of the Samples

The samples were irradiated 24 h after the gel preparation by Linear Accelerator to 6 MV X-ray (Siemens company- Germany) and in the field dimension of 20×20 cm in gantry angle of 60°. The vials were placed in cuboid water phantom (source-to-surface distance=95 cm). They were irradiated at the doses of 0.5 Gy, 1.5 Gy, 2.5 Gy, 4 Gy, and 6 Gy. Thenceforth, they were read-out by MRI system and sent to our laboratory for reading-out by OCT scanner.

For reading-out, first we light up the light source, CCD, and computer. The system was used after 10 min to allow the camera to warm up. The gel vial was installed on the stepper motor and room light was turned off. Then, we operated the stepper motor and the first projection was cached by the capture card. First rotation was done in 1°; and after 1 s, another rotation was done and the next projection obtained.

This process continued until the 360° was completed. The obtained data were sent to personal computer for processing and rebuilding images with MATLAB software (inverse-radon order).

Results

To read-out gel with Magnetic Resonance Imaging

For reading-out the gel, the optimum time was 24 h after irradiating, because monomers in the gel should be completely converted to polymer. There was a linear relationship between the magnetic resonance relaxation rate and the absorbed dose at a point in the dosimeter gel. By drawing the map of the relaxation rates, it was possible to achieve the dose by calculation and appropriate calibration. In MRI, a radio wave or frequency pulse hits the object and the signal is received from the magnetized spin (proton) on the object. Images are formed using spin relaxation times. When two spins are next to each other, the magnetic field of a proton influences the other proton. The magnetic field difference created by the interaction of a proton-proton may be very small; however, it causes the uniformity of the magnetic field spins to be exposed. This interaction is an intrinsic property of any object, which is measured by T_2 , and is known as the spin-spin or transverse relaxation time.

Inverse T_2 ($R_2 = \frac{1}{T_2}$) is called relaxation rate, using

which the amount of absorbed dose is calculated. One of the methods for extracting R_2 is a multi-point method whose R_2 map is obtained by fitting the MRI signals in different echoes using the equation $S = S_0 \exp(-R_2 T E)$. S_0 is the time signal for zero echo. For obtaining R_2 of images, a succession of spin-echo was done with 16 echo and time difference of 22 s using standard head coil. The protocol of this imaging is demonstrated in Table 4. For calculating R_2 , images were sent to a personal computer. Image processing was done in MATLAB software. Relaxation rate R_2 was done pixel to pixel. The linear decay curve was fitted by using obtained data. For obtaining calibration curve, R_2 was fitted in terms of dose and by use of this calibration curve, R_2 images were converted to dose maps. The result of measurement of gel vials for calibration is shown in Figure 6. Data for these results were shown in Table 5. In obtained images from MRI for every vial, R_2 number is an average field of view.

Table 4. Protocol of MRI Imaging in this study

| Field of view (mm) | TE (ms) | TR (repeat Time) (Sms) | Slice Thickness (mm) | Matrix size | Voxel size (mm) | NEX | Number of slice |
|--------------------|---------|------------------------|----------------------|-------------|-----------------|-----|-----------------|
| 320 | 22-352 | 3000 | 3 | 320×320 | 3×3×1 | 3 | 5 |

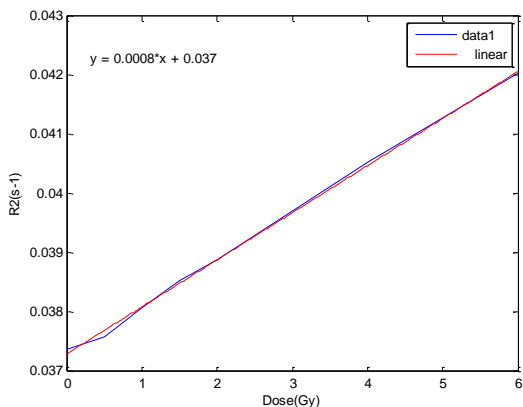


Figure 6. Calibration curve for MAGIC-f gel in magnetic resonance imaging

Table 5. The corresponding numbers of MAGIC-f gel in magnetic resonance imaging

| Dose(Gy) | R2(s ⁻¹) |
|----------|----------------------|
| 0 | 0.03737 |
| 0.5 | 0.03758 |
| 1 | 0.03808 |
| 1.5 | 0.03853 |
| 2 | 0.03888 |
| 4 | 0.04035 |
| 6 | 0.04204 |

Figure 6 is illustrated using the data of Table 5. Because there is a linear relationship between R₂ and dose amount, we fitted the linear diagram from data in Figure 6 (red line). The indicative equation of this linear diagram is Equation 3. Afterwards, we used this equation for obtaining the unknown dose amount and comparing with OCT data.

$$Y = 0.0008x + 0.037 \tag{3}$$

Y shows light attenuation and x shows the dose amount.

To Read-out Gel for Optical Coherence Tomography System

According to the results, the opacity of the gel increased by increasing dose amount, then we can survey this by the use of densitometer, technically, or eye, theoretically. Due to the increase of the opacity of the gel by irradiation, we can obtain 2D images from dose distribution by use of optical scan. Light attenuation is proportional with polymer density and absorbed dose. We can use this property and obtain data in Table 4.

By increasing absorbed doses, the opacity of monomer polymerization increased. For drawing

calibration curve, light attenuation amount was obtained in cut-out of gel vials with different doses (Figure 7).

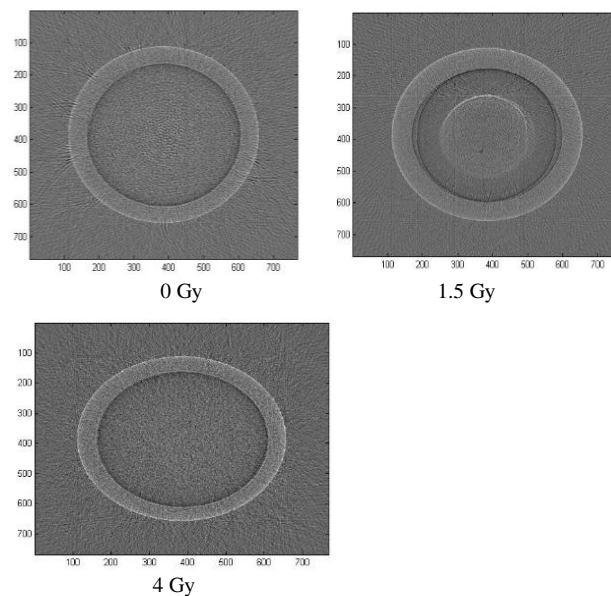


Figure 7. Rebuilt images samples cut out images in optical coherence tomography

Table 6. The corresponding numbers of MAGIC-f gel in optical coherence tomography

| Dose(Gy) | Light attenuation |
|----------|-------------------|
| 0 | 0.03135 |
| 0.5 | 0.03348 |
| 1 | 0.03548 |
| 1.5 | 0.03781 |
| 2 | 0.04125 |
| 4 | 0.04778 |
| 6 | 0.05743 |

The results of the measurements of the gel for calibration and the corresponding numbers are shown in Table 6 and Figure 8. The horizontal axis shows the dose amount and the vertical axis shows the light attenuation. In the obtained images from the OCT scanner, light attenuation was obtained for every tube.

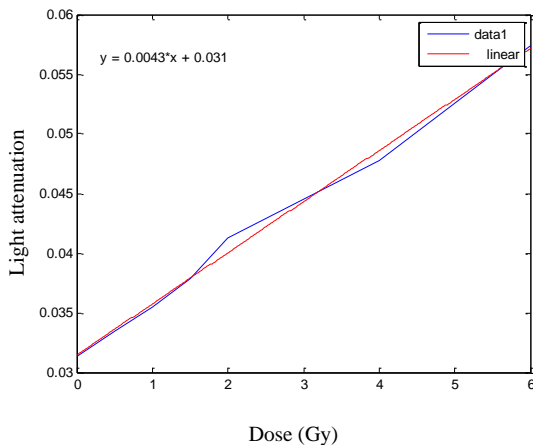


Figure 8. calibration curve for MAGIC-f gel in optical coherence tomography

Due to the fact that light attenuation is a linearity function with dose amount, we could fit the red diagram in Figure 8 and obtain Equation 4:

$$Y = 0.0043x + 0.031 \quad (4)$$

where Y shows light attenuation and x is the dose amount.

For comparing read-out Images with MRI and OCT, we irradiated a gel vial with X-ray dose amount and we scanned these vials with MRI and OCT. Then we obtained R_2 number and light attenuation by use of inverse radon code. The R_2 and light attenuation were considered to be 0.03856 and 0.03943, respectively. By replacing R_2 in Equation 1 and light attenuation in Equation 2, we obtained $x=2$ (dose amount) for MRI and $x=1.96$ for OCT system. Moreover, the dose amount for MRI was obtained as 2 and 1.96 for OCT. Then the error number dose of OCT to MRI can be obtained as following (Equation 5):

$$\text{Error number} = \frac{2-1.96}{2} \times 100 = 2\% \quad (5)$$

This error for OCT is acceptable in comparison to MRI.

The advantages of the optical imaging technique are being easily accessible, cost-effectiveness, and having high spatial resolution. Although the MRI method is the standard reading method, there is a significant limitation in the use and access to these systems such as being expensive and no access to MRI for gel dosimetry for radiotherapy departments to perform a gel dosimetry.

An external sample of a computerized OCT is available in two models of fan and pencil beam on the world market for dosimetric purposes; nevertheless, it is not possible to purchase this system for the radiotherapy department due to the mentioned limitations. The only sample of this system was built in Tabriz, Iran, 2012. Sample scanning was performed using lasers and photodiodes that are not economically feasible. The system we developed in this study was an LED- and CCD-based system that has the ability to scan 3D samples in less time.

This system is in line with the latest generation of optical computing in the global market. Our goal was to design and construct an optical system for fast and accurate dose reading by examining the parameters and comparing it with MRI.

Discussion

Considering the need for radiotherapy to confirm the distribution of absorbed dose of complex fields by dosimeter gel, this study was conducted to design an optical computed tomography system for using in radiotherapy dosimetry. Formerly, an MRI system was used for dosimetry; however, it was expensive and time-consuming. In the OCT system, these disadvantages were been resolved.

The OCT systems are two types including CCD- and photodiode-based systems. Unlike the CCD-based systems, the photodiode-based ones require two transitions and rotation motions to repeat each projection, which increases the scanning time. The system of this study is of the CCD type. Reducing the scanning time is a very important advantage of this system in comparison to the photodiode-based systems (Zakariaee, Mesbahi, Keshtkar, and Azimirad, 2014). In a study performed on a computed tomography scan system in 2005, the spatial resolution was about 2 mm and the scanning time was about 7 min (Van Doorn, Bhat, Rutten, Tran, and Costanzo, 2005). In another study carried out in 2011, the scanning time was calculated to be about 30 min (Olding and Schreiner, 2011). In this study, the spatial resolution of the OCT system was about 0.27 mm and the scanning time was about 6 min, which were important advantages of the system.

Conclusion

In this study, MRI was regarded as a gold standard method and OCT scanner was compared with MRI. The specific doses of 2 Gy in MRI and 1.96 Gy in OCT, which were very near to the real dose amount, were obtained. The error was 2%, which is negligible in experimental work. Therefore, it can be concluded that we can use our OCT system instead of MRI with the negligible error.

The aim of the project was to create a fast and accurate optical system for reading dose distribution. The best advantage of this system is the low scanning time. For showing this property we compared our OCT system with an approximately similar system in Tabriz University. In their system, they used laser instead of LED and photocell instead of CCD; therefore, a horizontal motion for vials was added to horizontal motion system in comparison to our system that only had a vertical motion. In practice in their system scanning time was more than that of our system. By building this system, gel dosimetry can be performed without any need to MRI. By the application of this system, we can improve the treatment of patients and increase the quality of radiotherapy. The proper function of this system was checked by using several dosimetry

parameters such as repeatability, spatial resolution, and uniformity. This system with the algorithm employed was able to reconstruct images and obtain cross-sectional images of slices. The function accuracy of this system was surveyed by comparison with MRI and by our OCT scanner, we can perform gel dosimetry independently from MRI. In conclusion, by applying this OCT system in radiotherapy dosimetry, we can improve the quality of therapy.

Acknowledgment

Authors would like to thank the University of Mazandaran for their support of this project.

References

1. De Deene Y, De Wagter C, Van Duyse B, Derycke S, De Neve W, Achten E. Three-dimensional dosimetry using polymer gel and magnetic resonance imaging applied to the verification of conformal radiation therapy in head-and-neck cancer. *Radiotherapy and Oncology*. 1998 Sep 1;48(3):283-91.
2. Oldham M, Siewerdsen JH, Shetty A, Jaffray DA. High resolution gel-dosimetry by optical-CT and MR scanning. *Medical physics*. 2001 Jul 1;28(7):1436-45.
3. Doran SJ, Koerkamp KK, Bero MA, Jenneson P, Morton EJ, Gilboy WB. A CCD-based optical CT scanner for high-resolution 3D imaging of radiation dose distributions: equipment specifications, optical simulations and preliminary results. *Physics in Medicine & Biology*. 2001 Nov 14;46(12):3191.
4. Gore JC, Ranade M, Maryanski MJ, Schulz RJ. Radiation dose distributions in three dimensions from tomographic optical density scanning of polymer gels: I. Development of an optical scanner. *Physics in Medicine & Biology*. 1996 Dec;41(12):2695.
5. Hiltz M, Audet C, Duzenli C, Jirasek A. Polymer gel dosimetry using x-ray computed tomography: a feasibility study. *Physics in Medicine & Biology*. 2000 Sep 1;45(9):2559.
6. Maryanski MJ, Zastavker YZ, Gore JC. Radiation dose distributions in three dimensions from tomographic optical density scanning of polymer gels: II. Optical properties of the BANG polymer gel. *Physics in Medicine & Biology*. 1996 Dec;41(12):2705.
7. Lopatiuk-Tirpak O, Langen KM, Meeks SL, Kupelian PA, Zeidan OA, Maryanski MJ. Performance evaluation of an improved optical computed tomography polymer gel dosimeter system for 3D dose verification of static and dynamic phantom deliveries. *Medical physics*. 2008 Sep 1;35(9):3847-59.
8. Mather ML, Baldock C. Ultrasound tomography imaging of radiation dose distributions in polymer gel dosimeters: Preliminary study. *Medical physics*. 2003 Aug 1;30(8):2140-8.
9. Oldham M. 3D dosimetry by optical-CT scanning. In *Journal of Physics: Conference Series 2006* (Vol. 56, No. 1, p. 58). IOP Publishing.
10. Clift C, Thomas A, Adamovics J, Chang Z, Das I, Oldham M. Toward acquiring comprehensive radiosurgery field commissioning data using the PRESAGE®/optical-CT 3D dosimetry system. *Physics in Medicine & Biology*. 2010 Feb 4;55(5):1279.
11. Olding T, Holmes O, Schreiner LJ. Cone beam optical computed tomography for gel dosimetry I: scanner characterization. *Physics in Medicine & Biology*. 2010 Apr 22;55(10):2819.
12. Olding T, Schreiner LJ. Cone-beam optical computed tomography for gel dosimetry II: imaging protocols. *Physics in Medicine & Biology*. 2011 Feb 1;56(5):1259.
13. Ikeda M, Nakano Y. Spectral luminous-efficiency functions obtained by direct heterochromatic brightness matching for point sources and for 2 and 10 fields. *JOSA A*. 1986 Dec 1;3(12):2105.